CrystEngComm

ROYAL SOCIETY
OF CHEMISTRY

PAPER
Consiglia Tedesco, Irene Izzo *et al.*
Ring size effect on the solid state assembly of propargyl substituted
hexa- and octacyclic peptoids

175 YEARS

CrystEngComm

Ring size effect on the solid state assembly of propargyl substituted hexa- and octacyclic peptoids†

Consiglia Tedesco,*[a] Alessandra Meli,[a] Eleonora Macedi,[a] Veronica Iuliano,[a] Antonio G. Ricciardulli,[a] Francesco De Riccardis,[a] Gavin B. M. Vaughan,[b] Vincent J. Smith,[c] Leonard J. Barbour[c] and Irene Izzo*[a]

The investigation of the solid state assembly of propargyl substituted hexa- and octacyclic peptoids highlights the effect of ring size in determining the packing arrangement of the macrocycles. A layered arrangement is obtained in the case of the hexacyclic peptoid **1** and a tubular arrangement in the case of the octacyclic peptoid **2**. Guest molecules either intercalate between the layers as in **1** or are located within the peptoid nanotube as in **2**.

Introduction

The growing interest in natural and synthetic macrocycles involves heterogeneous areas of science. Biochemistry, crystal engineering, supramolecular chemistry, catalysis and material science lead the way in the discovery of new annulated structures and their intriguing properties.[1]

The importance of cyclic peptoids to these various areas is owing to the abundant chemical properties as well as their unexpected biological activity.[2] In general, peptoids differ from peptides in the position of the side chains, which is shifted by one position along the peptide backbone to give *N*-substituted oligoglycines (Fig. 1).[3]

The lack of amide protons prevents the formation of NH···OC hydrogen-bonds, but does not hamper the formation of helical or ribbon-like secondary structures, that are often driven by weak interactions.[4]

The almost isoenergetic *cis/trans* conformations of tertiary amide bonds add further flexibility to the peptoid backbone (when compared to the corresponding peptide, Fig. 2). The introduction of sterically bulky, α-chiral and aryl side chains and/or backbone cyclization represent useful strategies for inducing conformational rigidity.[2,4] Cyclic peptoids may en-

code reverse-turn type secondary structures and therefore interfere with critical protein–protein interactions.[2i,2m]

Cyclic peptoids are very versatile building blocks for the assembly of solid state supramolecular architectures, because the desired specific interactions may be provided by a variety of functional side groups attached to a sizeable scaffold.[5]

In a recent survey of the solid state assembly of free and metal coordinated cyclic α-peptoids[5] we were able to identify many common features recurring in the aggregation of cyclic α-peptoids. Weak interactions, such as weak hydrogen bonds or CH–pi interactions, play a key role.[6,7]

Inter-annular CH···OC hydrogen bonds can provide either face-to-face or side-by-side arrangements of the macrocycles embodying the peptoid counterpart of β-sheet secondary structure in proteins.[2g,2k,5] As previously stated,[5] side chains strongly influence the solid state assembly of peptoid macrocycles. N-linked benzyloxyethyl residues (arrayed horizontally with respect to the macrocycle plane) promote a face-to-face columnar arrangement of the macrocycles,[2k] inducing the formation of a peptoid nanotube. The interannular CH···OC hydrogen bonds replace the NH···OC hydrogen bonds found in the case of alternate D–L peptide nanotubes as described by Ghadiri.[8]

Side chains may also act as pillars by inducing a columnar arrangement of peptoid macrocycles: methoxyethyl and propargyl side chains are able to extend vertically with

[a] Department of Chemistry and Biology "A. Zambelli", University of Salerno, Via Giovanni Paolo II 132, 84084 Fisciano (SA), Italy. E-mail: ctedesco@unisa.it, iizzo@unisa.it

[b] European Synchrotron Radiation Facility, 8 Rue J. Horowitz, 38043 Grenoble, France

[c] Department of Chemistry and Polymer Science, University of Stellenbosch, Private Bag X1, 7602 Matieland, Stellenbosch, South Africa
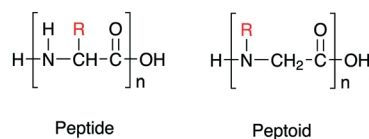
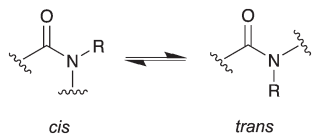Fig. 1 Comparison between peptide and peptoid structures.

Fig. 2 *Cis/trans* conformational isomerism in tertiary amides.

respect to the macrocycle plane and interact with the backbone atoms belonging to the macrocycles below and above.[2g,9]

Also, the size of the macrocycle may have a considerable effect on the solid state arrangement: as the ring size increases side-by-side and/or columnar ordering is favoured.

The occurrence of hydrate or solvate forms among cyclic peptoids is rather common. Guest molecules are key components of the crystal architecture of cyclic peptoids.[2i,2m,10] Sometimes the guest molecules can be removed with preservation of the single crystal habit, as recent examples of a highly thermostable cyclic octamer[9] and an acetonitrile inclusion compound of a substituted cyclohexamer with four propargyl and two methoxyethyl side chains have shown.[11]

With the aim of better understanding the influence of ring size on the solid state assembly of cyclic peptoids, we report herein the crystal structures of fully propargylated hexameric and octameric cyclic peptoids (**1** and **2**, Fig. 3). Using Hirshfeld surface analysis, which quantitatively summarizes the nature and kind of molecular interactions experienced by a molecule in a crystal,[12] we relate the different inclusion properties of the two cyclic peptoids to the solid state supramolecular architecture.

Results and discussion

The syntheses of the cyclic hexamer, cyclo-(Npa)$_6$ **1**, and of the cyclic octamer, cyclo-(Npa)$_8$ **2**, have been previously reported.[13] In order to obtain crystals suitable for X-ray diffraction analysis we attempted several crystallization trials.

From the slow evaporation of an acetonitrile solution we obtained the crystal form **1A** and from the slow evaporation of a DMSO/water/acetonitrile solution the crystal form **1B**.

The X-ray crystal structure of **1A** corresponds to an acetonitrile solvate with a 1:2 host:guest ratio between the cyclopeptoid and acetonitrile molecules. The unit cell contains 2 cyclopeptoid molecules and 4 acetonitrile molecules.
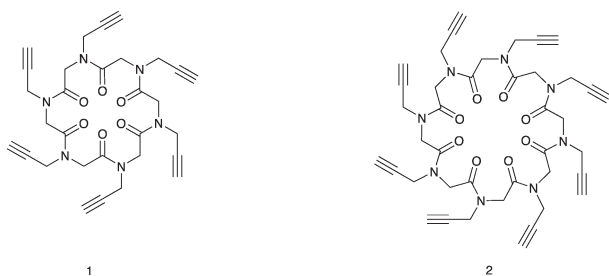

Fig. 3 Cyclo-(Npa)$_6$ **1** and cyclo-(Npa)$_8$ **2**, Npa = *N*-(propargyl)glycine.

Table 1 Crystal data and structural refinement details for cyclo-(Npa)$_6$ solvates **1A** and **1B**

	1A	1B
Formula	$C_{30}H_{30}N_6O_6 \cdot 2CH_3CN$	$C_{30}H_{30}N_6O_6 \cdot 2DMSO \cdot 2H_2O$
Formula weight	652.71	762.89
System	Monoclinic	Monoclinic
Space group	$P2_1/c$	$P2_1/c$
a (Å)	11.717(6)	13.022(2)
b (Å)	17.333(9)	17.377(3)
c (Å)	8.824(5)	8.6788(15)
β (°)	106.290(6)	102.255(4)
V (Å^3)	1720.1(16)	1919.1(6)
Z	2	2
D_X (g cm^{-3})	1.260	1.320
μ (mm^{-1})	0.056	0.201
F_{000}	688.0	808.0
Wavelength (Å)	0.29520	0.71073
R ($I > 2\sigma_I$)	0.0678(4038)	0.1145(2202)
$_wR_2$ (all)	0.2189(4708)	0.3630(4720)
N. of param.	218	237
GooF	1.113	1.003
$\Delta\rho$ min/max (e Å^{-3})	−0.36/0.59	−1.11/0.94

The X-ray crystal structure of **1B** is also a solvate with a 1:2:2 host:guest ratio between cyclopeptoid, DMSO and water molecules. The unit cell contains 2 cyclopeptoid molecules, 4 DMSO and 4 water molecules.

Relevant crystallographic data and structure refinement details are listed in Table 1 for both forms **1A** and **1B**. In both forms the macrocycle possesses a crystallographic inversion centre and exhibits a distorted *cctcct* (*c* = *cis* and *t* = *trans*) conformation of the peptoid backbone, with two propargyl side chains pointing vertically up and down with respect to the macrocycle plane and four propargyl side chains extending horizontally in the equatorial direction (Fig. 4 and S1 ESI†).

The peptoid backbone atoms of forms **1A** and **1B** overlay almost perfectly (rmsd 0.064 Å). Slight differences are due to the side chain orientations (Fig. 5a), indeed the molecular structure overlay is within a rmsd of 0.226 Å.
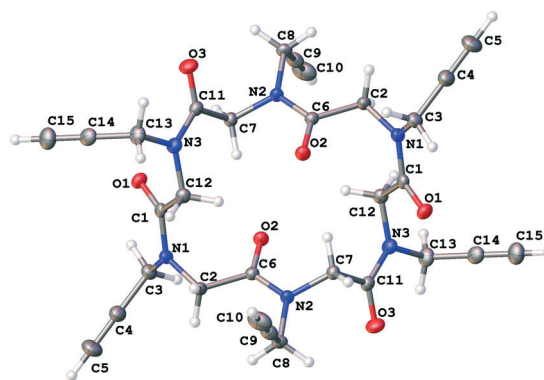

Fig. 4 ORTEP with labelling scheme for the cyclopeptoid molecule in crystal form **1A**. The same labelling scheme is adopted in crystal form **1B** (Fig. S1 ESI†).
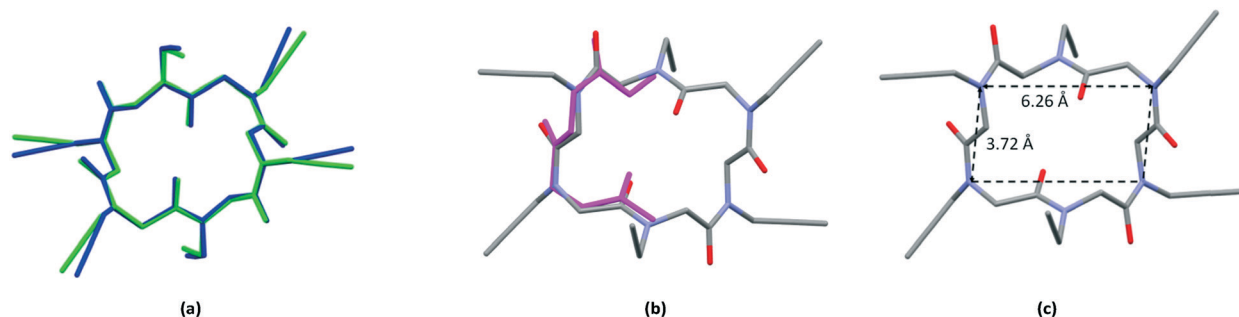
Fig. 5 (a) Peptoid backbone overlay between crystal forms **1A** (blue) and **1B** (green), rmsd 0.064 Å. (b) Superposition of the backbone atoms of the cyclopeptoid molecule in crystal form **1A** with idealized type III β-turn peptide (magenta), rmsd 0.344 Å (see Fig. S2b ESI† for **1B** superposition). (c) Rectangular shape of cyclic peptoid backbone in crystal form **1A**. Four *cis* amide bonds reside at each corner, *trans* amide bonds are located on two opposing sides. Values for the rectangular length and width are also reported.

The propensity to mimic reverse turn secondary structures in proteins[2i,2m] was tested by the superposition of the peptoid backbone atoms (N2, C6, C2, N1, C1, C12, N3, C11, C7, and N2) respectively in **1A** and **1B** with the corresponding peptide backbone atoms (Cαi, Ci, Ni + 1, Cαi + 1, Ci + 1, Ni + 2, Cαi + 2, Ci + 2, Ni + 3, and Cαi + 3) of idealized β-turns, types I and III,[14] corresponding rmsd values are reported in Table 2.

The peptoid backbone seems to adapt better to a type III β-turn structure, in which the N-linked side chains are located in the same position as the Cα-linked side chains in peptides (Fig. 5b and S2 ESI†).

The rectangular shape of the macrocycle is defined by the four nitrogen atoms at the corners (where the horizontal propargyl side chains are located) and two parallel short and long sides (Fig. 5c and S3 ESI†).

As shown in Fig. 6, the crystal structures of both forms **1A** and **1B** assemble in the *bc* plane forming layers of cyclopeptoid molecules intercalated by guest molecules.

The dominant packing interactions were assessed by Hirshfeld surface analysis (Fig. 7, 8 and S4 ESI†) and can be divided into two types: intra- and interlayer interactions. In both crystal forms the layers of the cyclopeptoid molecules originate from side-by-side interannular CO⋯H$_2$C interactions along the short sides of the rectangular macrocycles (Fig. 7), which are interlinked by means of the *cis* carbonyl oxygen atom O1 and the backbone methylene hydrogen atom C12 (CO⋯HC distance is 2.18 Å and O⋯HC angle is 166.7° in form **1A**, CO⋯HC distance is 2.23 Å and O⋯HC angle is 157.5° in form **1B**).

The vertical side chains help stabilize the layers by means of CO⋯HC≡C interactions between the terminal hydrogen atom and the oxygen atom O1 (CO⋯HC distance 2.34 Å, O⋯HC angle 153.0° in form **1A** and CO⋯HC distance 2.34 Å, O⋯HC angle 143.8° in form **1B**).

Horizontal side chains C13–C14–C15 also contribute to the stability of the layers by means of an intricate interlace of CH⋯OC and CH–pi interactions (Fig. S5a and b ESI†).

In the case of the crystal form **1A** horizontal side chains C13–C14–C15 are also involved in pi–pi interactions with the vertical side chains C8–C9–C10 of neighbouring cyclopeptoid molecules (Fig. S5a ESI†). In **1A** the horizontal side chains C3–C4–C5 interconnect the layers through CO⋯HC≡C interactions involving the *cis* carbonyl oxygen atoms O3 (CO⋯HC 2.18 Å, O⋯HC angle 158.4°).

In form **1B** the same horizontal side chains C3–C4–C5 and the *cis* carbonyl oxygen atoms O3 are bridged by a water molecule, connecting the cyclopeptoid layers (C≡CH⋯O 2.18 Å, O⋯OC 2.83 Å, Fig. 8).

The guest molecules, either acetonitrile or DMSO and water molecules, occupy the void space between the layers (Fig. S6 ESI†).

In **1A**, acetonitrile molecules interact with the host by means of CH⋯OC hydrogen bonds and CH–pi interactions. In the case of **1B**, water molecules interact with the host as previously described and also act as a bridge between DMSO and the host molecules. The DMSO molecule connects two layers by means of CH–pi interactions between the methyl hydrogen atoms and the pi system of the horizontal side chains (CH⋯C 2.75 Å, CH⋯C 2.82 Å).

In both forms the layers of cyclopeptoid molecules alternate with guest molecules (along the *a* axis). In form **1B** the *a* axis is longer than in **1A** as a consequence of the different size and type of the guest molecules, thus the gap between the cyclopeptoid layers can be tuned by the guest molecules.

Hirshfeld fingerprint plots for **1A** and **1B** in Fig. 9 emphasize the nature of the interactions and their quantitative contributions towards the crystal packing.

For **1A** the symmetric sharp spikes pointing towards the bottom left corner of the plot correspond to CH⋯OC contacts between cyclopeptoid molecules. The wings on either

Table 2 Superposition of peptoid backbone atoms with idealized β-turns peptide backbone atoms

	1A rmsd (Å)	1B rmsd (Å)	2A rmsd (Å)
Idealized type I β-turn	0.434	0.473	0.437
Idealized type III β-turn	0.344	0.369	0.359

Peptoid backbone atoms (N2, C6, C2, N1, C1, C12, N3, C11, C7, and N2) in crystal forms **1A**, **1B** and peptoid backbone atoms in crystal form **2A** (N4, C16, C12, N3, C11, C7, N2, C6, C2, N1) are overlaid with the corresponding peptide backbone atoms (Cαi, Ci, Ni + 1, Cαi + 1, Ci + 1, Ni + 2, Cαi + 2, Ci + 2, Ni + 3, and Cαi + 3) of idealized type I and III β-turns.
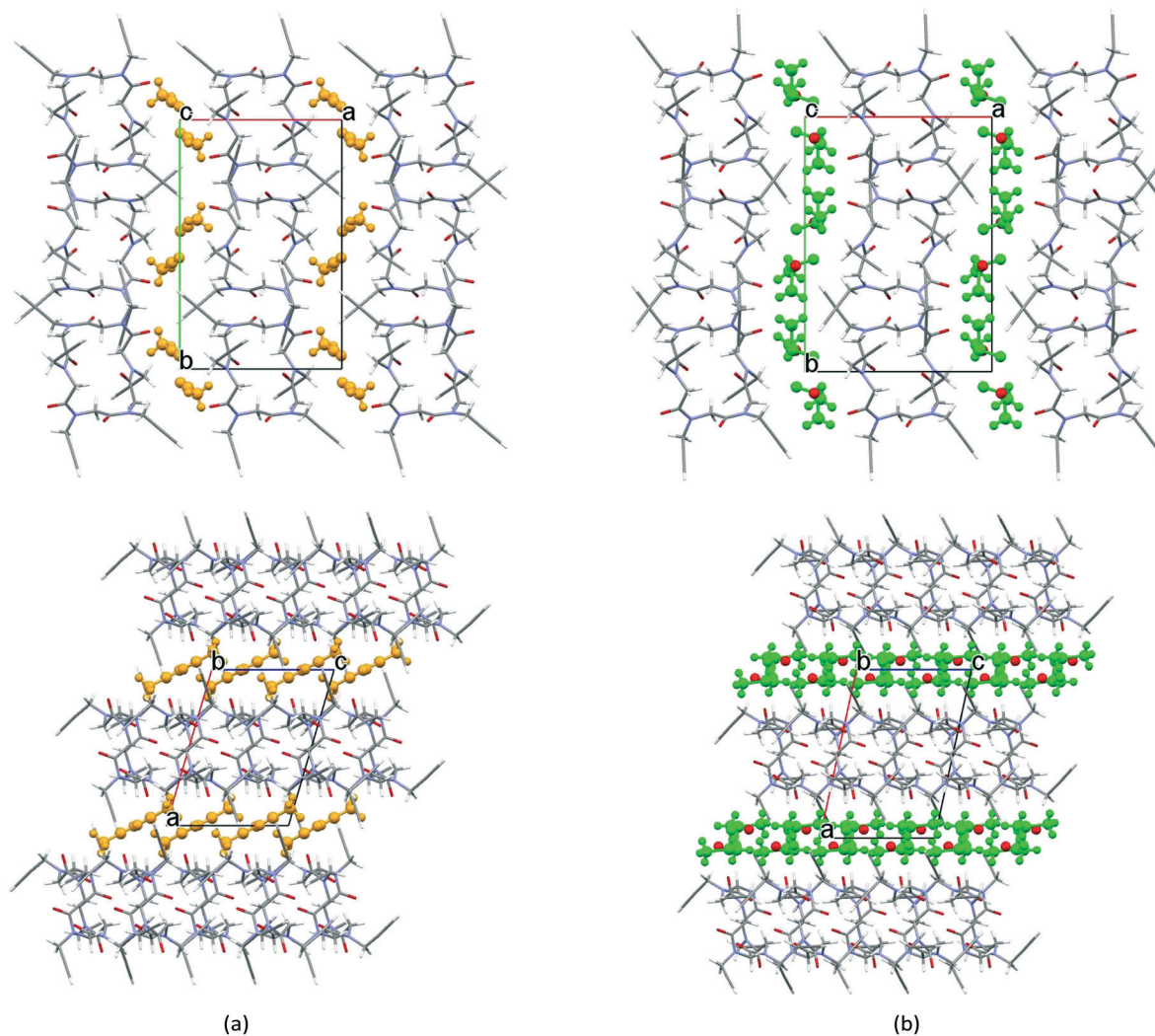
Fig. 6 (a) Crystal packing of the crystal forms **1A** (a) and **1B** (b) as viewed along the *c* (top) and *b* (bottom) axes. Guest molecules are depicted in ball-and-stick style with the acetonitrile molecules in yellow, water molecules in red and DMSO molecules in green.

side of the diagonal are indicative of CH–pi interactions (Fig. 9). The bottom right wing features a light blue area, not present in the upper left wing and these are due to CH–pi host–guest interactions. The upper central blue spike corresponds to loose H⋯H contacts in the crystal packing.

For **1B** host–guest interactions are represented by the asymmetry in the bottom sharp spike and wing. The former is due to water-mediated interlayer interactions, the latter to CH–pi contacts provided by the DMSO molecules. The upper central blue spike accounts for loose C⋯H and H⋯H contacts.

Suitable crystals for the cyclooctamer **2** were obtained by slow evaporation of methanol solutions and were flash-cooled before measuring. The X-ray crystal structure corresponds to a methanol solvate indicated as crystal form **2A**, with a 1:2 host:guest ratio between the cyclopeptoid and methanol molecules. There are 4 cyclopeptoid molecules and 8 methanol molecules in the unit cell. Crystal data

and structure refinement details for **2A** are reported in Table 3.

The macrocycle possesses a crystallographic two-fold axis and exhibits a distorted *ccttcctt* conformation of the peptoid backbone. Four side chains point vertically up and down with respect to the macrocycle plane, while four propargyl side chains extend horizontally (Fig. 10).

The propensity of the cyclic octamer to mimic reverse turn secondary structures in proteins[2i,2m] was tested by the superposition of the peptoid backbone atoms of **2A** (N4, C16, C12, N3, C11, C7, N2, C6, C2, N1) with the corresponding peptide backbone atoms (Cαi, Ci, Ni + 1, Cαi + 1, Ci + 1, Ni + 2, Cαi + 2, Ci + 2, Ni + 3, and Cαi + 3) of idealized type I and III β-turns.[14] The corresponding rmsd values are reported in Table 2. The peptoid backbone seems to adapt better to a type III β-turn structure, in which the N-linked side chains are located in the same positions as the Cα-linked side chains in peptides (ESI† Fig. S7).
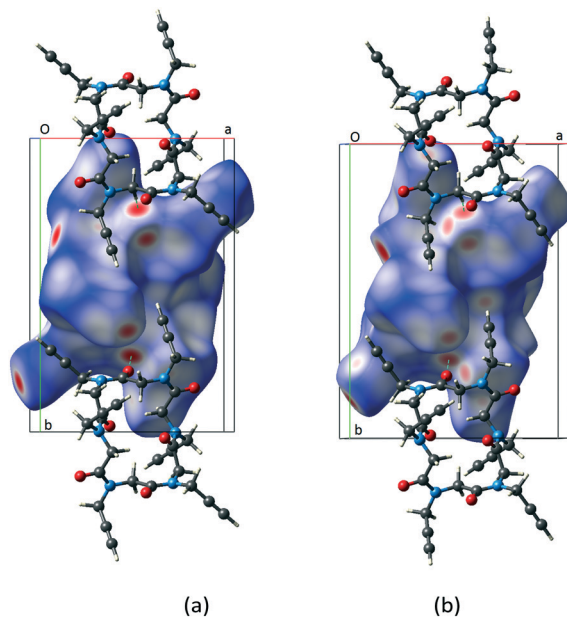
(a)   (b)

Fig. 7 Hirshfeld surface of the cyclopeptoid molecule in crystal forms **1A** (a) and **1B** (b) as viewed along the *c* axis. Side by side interannular CO···H₂C interactions along the short sides of the backbone macrocycles are highlighted by green dotted lines.

In **2A** the cyclopeptoid molecules align along the shortest axis (*c* axis) in a tubular architecture, forming hollow cavities, where the guest molecules are located (Fig. 11a, 12 and S8 ESI†).

As highlighted by the Hirshfeld surface analysis, the key interactions among the cyclopeptoid molecules in **2A** can be divided into intratubular and intertubular interactions. As

shown in Fig. 11a and 13, the vertical side chains are mainly involved in the intratubular interactions that bind the peptoid backbone *trans* carbonyl oxygen atoms O2 and O4, through CO···HC hydrogen bonds (CO···HC≡C 2.17 Å, O···HC angle 156.1°, CO···HC≡C 2.26 Å, O···HC angle 169.6°).

The peptoid nanotubes are interconnected *via* side-by-side interannular CO···H₂C hydrogen bonds, which run along the long sides of the rectangular macrocycles (CO···HC 2.23 Å, O···HC angle 169.9°). These interactions involve the *cis* carbonyl oxygen atom O1 and the C12 backbone methylene hydrogen atom. Horizontal side chains C8–C9–C10 and C13–C14–C15 are involved in the intertubular interactions *via* CH–pi interactions (CH₂··· C≡C 2.75 Å, CH··· C≡C angle 142.6°).

Two methanol molecules per each cyclopeptoid molecule are located inside the nanotubes and are hydrogen bonded to the carbonyl oxygen atoms O4 (CO···O 2.78 Å, CO···HO 1.94 Å, O···HC angle 175.3°). The methanol molecules also partake in hydrogen bonding with the horizontal propargyl side chains C8–C9–C10 of neighbouring cyclopeptoids (C≡CH···OCH₃ 2.33 Å, O···H–C angle 144.7°). The methanol molecules act both as hydrogen donors and acceptors and are involved in the intertubular connections. The Hirshfeld surface in Fig. 13b highlights the role of the guest molecules in the intermolecular interactions in **2A**.

The Hirshfeld fingerprint plots of **2A** are reported in Fig. 9. The upper left spike is due to the intratubular CH···OC hydrogen bond between cyclopeptoid molecules (at 2.17 Å distance), while the lower right spike is due to OH···OC contacts, where the cyclopeptoid molecule acts as an H-bond acceptor for the methanol molecules (at a distance of 1.9 Å). The green-blue streak that appears at $d_i + d_e$ > 2.1 Å corresponds to intra and intertubular CH···OC
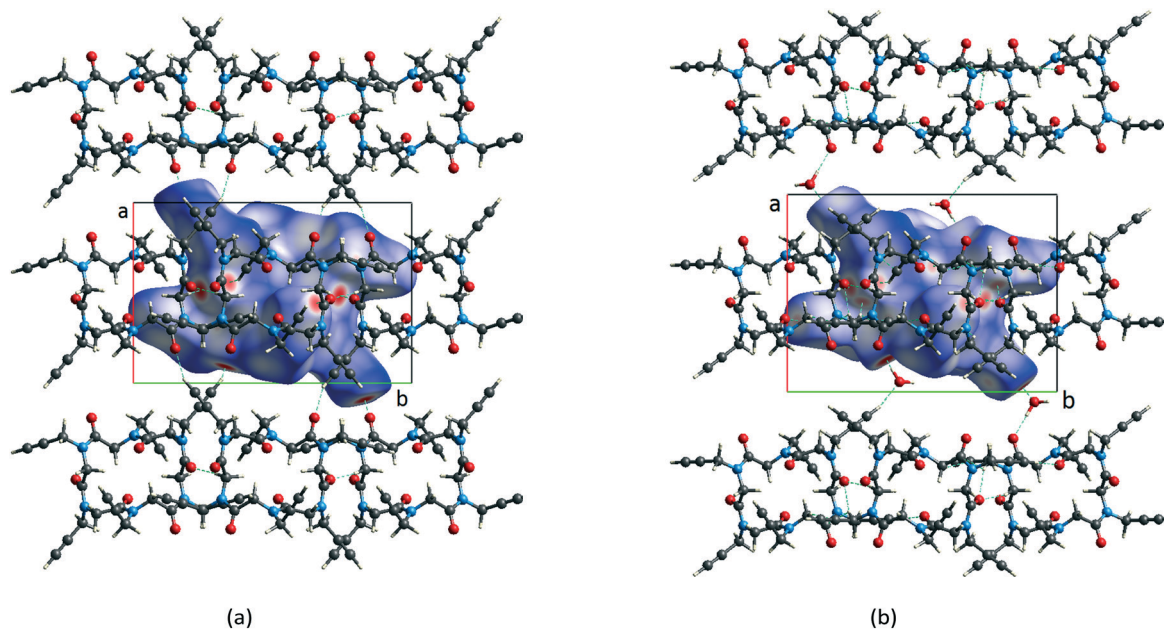

(a)   (b)

Fig. 8 Intra-layer and inter-layer interactions mapped onto the Hirshfeld surface of the cyclopeptoid molecule in crystal forms **1A** (a) and **1B** (b) both viewed along the *c* axis. Hydrogen bonds are highlighted by green dotted lines. For clarity DMSO molecules are omitted in figure (b).
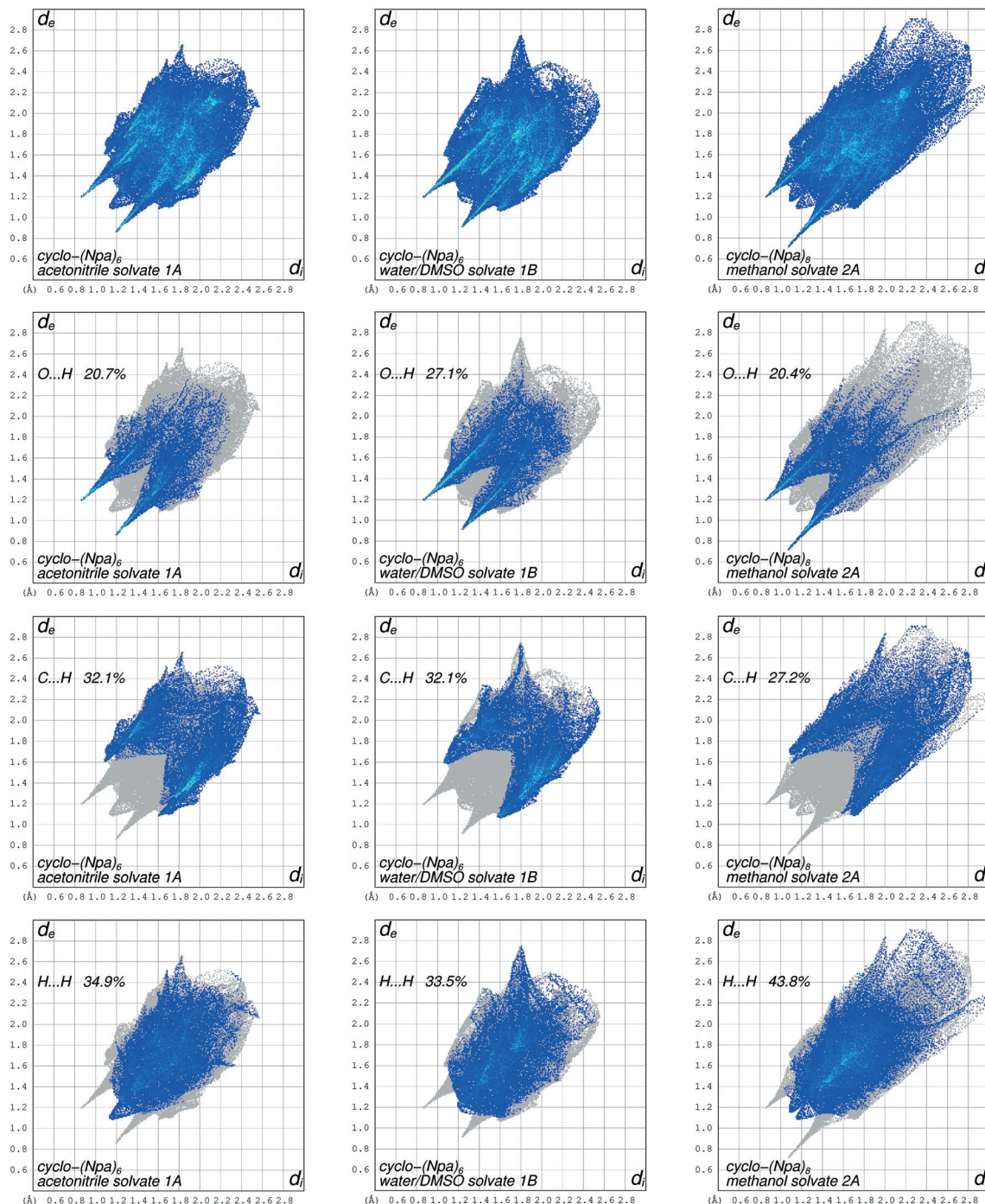
CrystEngComm

Fig. 9 Comparison of full and decomposed fingerprint plots of the crystal forms **1A**, **1B** and **2A**. The plots are decomposed into O⋯H, C⋯H and H⋯H intermolecular interactions. The full fingerprint appears beneath each decomposed plot as a grey shadow.

contacts (with the cyclopeptoid molecule as the H-bond acceptor). Notably the fingerprint plot of form **2A** in Fig. 9 extends beyond 2.8 Å for d_i and d_e values. The longer d_i and d_e values indicate a lower packing efficiency for the octacyclopeptoid **2A** than for the hexacyclopeptoid compounds **1A** and **1B**. The packing coefficients for **1A** and **1B** are 0.741 and 0.751 respectively, while the packing coefficient is 0.716 for **2A**.

It is noteworthy that the packing coefficient is 0.748 for the octacyclopeptoid previously reported by Kirshenbaum,[9]

cyclo-(Npa-Nme-Nph-Nph)$_2$, Nme = N-(methoxyethyl)glycine and Nph = N-(phenyl)glycine. This compound exhibits the same molecular geometry as **2A** and was crystallized from methanol as a hydrate form in the same space group $C2/c$. The cyclopeptoid molecules are also arranged in a tubular fashion. The cyclopeptoid nanotubes are filled with water molecules, that can be completely removed without disrupting the crystal architecture resulting in the apohost/ anhydrous form. As previously noted,[5,9] the water molecules

Table 3 Crystal data and structural refinement details for cyclo-(Npa)$_8$ **2** as crystal forms **2A**, **2B**, **2C** and **2D**

	2A	2B	2C	2D
Formula	$C_{40}H_{40}N_8O_8 \cdot 2CH_3OH$	$C_{40}H_{40}N_8O_8 \cdot CH_3OH \cdot 2H_2O$	$C_{40}H_{40}N_8O_8 \cdot 4H_2O$	$C_{40}H_{40}N_8O_8 \cdot 1.56CH_3OH \cdot 0.88H_2O$
Formula weight	824.88	828.87	832.86	826.58
System	Monoclinic	Monoclinic	Monoclinic	Monoclinic
Space group	$C2/c$	$C2/c$	$C2/c$	$C2/c$
a (Å)	29.138(11)	29.227(11)	29.250(12)	29.177(10)
b (Å)	8.033(2)	7.997(3)	7.997(3)	7.999(2)
c (Å)	21.635(8)	21.680(8)	21.648(9)	21.586(7)
β (°)	118.774(7)	119.615(7)	120.242(9)	119.075(7)
V (Å^3)	4439(3)	4405(3)	4375(3)	4403(2)
Z	4	4	4	4
D_X (g cm^{-3})	1.234	1.250	1.265	1.247
μ (mm^{-1})	0.090	0.092	0.095	0.091
F_{000}	1744.0	1752.0	1760.0	1748.0
Wavelength (Å)	0.71073	0.71073	0.71073	0.71073
R ($I > 2\sigma_I$)	0.0890 (2150)	0.0967 (3060)	0.1178 (1763)	0.1105 (2353)
$_wR_2$ (all)	0.2361 (5416)	0.2725 (5330)	0.3762 (5150)	0.3272 (5080)
N. of param.	273	277	266	278
GooF	0.977	1.063	0.988	1.083
$\Delta\rho$ min/max (e Å^{-3})	−0.29/0.26	−0.30/0.66	−0.33/0.56	−0.35/0.36

in the hydrate form are not involved in the intertubular interactions, which consist only of H-bond and CH–pi interactions, provided by the horizontal methoxyethyl and phenyl side chains, respectively.

Based on the observations that the Kirshenbaum analogue retains its single crystal habit upon dehydration, we decided to investigate the stability of the crystals of **2A** by changing the environmental conditions. During crystal manipulation we observed that the content and type of guest molecules changed when exposed to ambient humidity at room temperature.

A single crystal, mounted on a MiTeGen microloop™ in Paratone® N oil, was left for 15 minutes at room temperature. A partial exchange of methanol molecules with water molecules occurred resulting in the new form **2B**. The overlay of cyclopeptoid molecules **2A** and **2B** has an rmsd of 0.1325 Å (Fig. S9a ESI†). Moreover, crystal form **2B** is isostructural with

Fig. 10 ORTEP with numbering scheme for the cyclopeptoid molecule in crystal form **2A** as viewed along the *b* axis.

2A (Table 3 and Fig. S10 ESI†). The difference Fourier map reveals that each methanol molecule is partially substituted by two water molecules. One water molecule shares exactly the same oxygen site (O1S) with the methanol molecule and therefore replaces methanol as the hydrogen bond donor with respect to the same carbonyl oxygen atom O4. The other water molecule (O2S) completes the hydrogen bond network by bridging the previous water molecule (O1S), the carbonyl oxygen atom O3 and another symmetry equivalent water molecule (O2S in Fig. 11b). As shown by the least-squares refinement of the X-ray data the ratio between water molecules and methanol molecules in the crystal is 2 : 1.

To test the affinity of the cyclopeptoid for the water molecules and, in particular, to locate the crystal active sites for molecular recognition, a crystal of **2A** was soaked in distilled water for 24 h and flash-cooled to 100 K before measurement. This resulted in a completely hydrated form **2C**, where each methanol molecule is completely substituted by two water molecules (Fig. 11c). Cyclopeptoid molecules in forms **2C** and **2A** overlay within a rmsd value of 0.1956 Å (Fig. S9b ESI†). The hydrate form **2C** is isostructural with **2A** and **2B** (Table 3 and Fig. S10 ESI†).

As for the cyclopeptoid molecule, the carbonyl oxygen atoms O3 and O4 act as hydrogen bond acceptors and are the active sites for water molecule recognition. It must be noted that a certain degree of disorder exists with respect to the water molecule hydrogen bonded to the oxygen atom O3. This suggests that two methanol molecules fit better the void space in the cyclopeptoid tube than four water molecules.
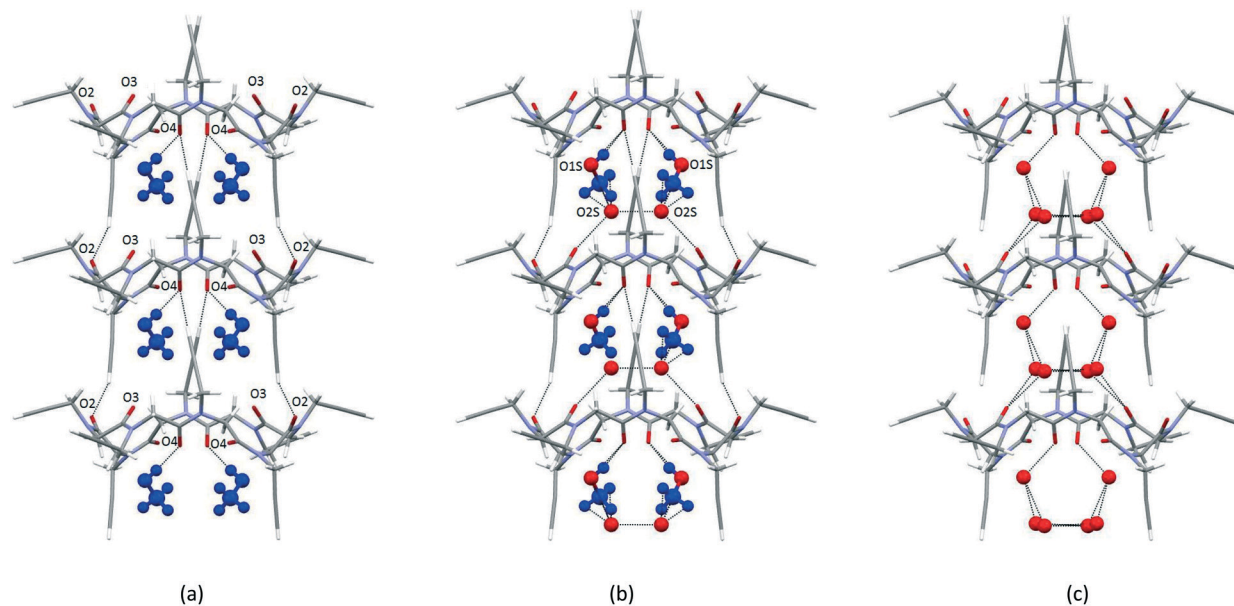
A competitive experiment was also performed by soaking a crystal of **2A** in a 50 : 50 (by volume) water : methanol solution for 3 h, obtaining the crystal form **2D**. Cyclopeptoid molecules in forms **2D** and **2A** overlay within an rmsd value of 0.0563 Å (Fig. S9c ESI†) and **2D** isostructural with **2A**, **2B** and **2C** (Table 3 and Fig. S10 ESI†).
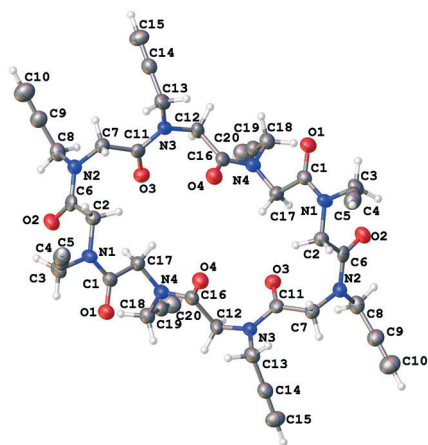
Fig. 11 Tubular arrangement of cyclopeptoid molecules in the crystal forms (a) **2A**, (b) **2B**, **2D** and (c) **2C** as viewed along the *c* axis. The shortest interactions are indicated as dotted lines. Guest molecules are depicted in ball-and-stick, methanol molecules in blue and water molecules in red. In the case of the crystal forms **2B** and **2D** each methanol molecule is partially substituted by two water molecules, one of these water molecules shares the oxygen site with the methanol molecule.

The hydrogen bonding network is the same as observed in **2B**, but methanol and water molecules have different occupancies (Fig. 11b). From the refinement of the structural data we determined that the water/methanol ratio had decreased to 0.56. This also suggests that methanol may be preferred with respect to water molecules. Crystal data and structure refinement details for forms **2B**, **2C** and **2D** are summarized in Table 3.

When we collected X-ray diffraction data on single-crystals of **2A** and **2C** stored at room temperature without surrounding mother liquor, we observed an increase in the mosaicity over time and after 24 h the quality of the diffraction images deteriorated beyond reliable indexing. We could therefore infer that the guest molecules help stabilize the crystal architecture (as indicated by Hirshfeld surface analysis, Fig. 13b) and that the guest molecules cannot be completely removed while preserving the crystal integrity. Water molecules from ambient humidity are not sufficient to replace the guest molecules in order to stabilize the crystal structure.

Experimental

Crystallization

Form 1A. Compound **1** (3.5 mg) was dissolved in 4 mL of hot acetonitrile and crystallized by slow evaporation. Colourless crystals were obtained as small needles, that were only suitable for synchrotron X-ray diffraction.

Form 1B. Compound **1** (1.5 mg) was dissolved in 300 μL DMSO, 300 μL H_2O and 2 mL acetonitrile and crystallized by slow evaporation as colourless hexagonal plates, that were suitable for a laboratory X-ray diffraction instrument.

Form 2A. Compound **2** (1.0 mg) was dissolved in 2 mL of hot methanol and crystallized by slow evaporation as colourless needle-like crystals, that were suitable for a laboratory X-ray diffraction instrument.

Soaking experiments

Crystals of **2A** were removed from the methanol solution and soaked in distilled water for 24 h (hydrate crystal form **2C**) and in a 50:50 by volume water/methanol solution for 3 h (crystal form **2D**). A crystal of **2C** (0.38 × 0.20 × 0.16 mm) and a crystal of **2D** (0.28 × 0.15 × 0.13 mm) suitable for laboratory X-ray diffraction were selected and mounted on a MiTeGen microloop™ with Paratone® N oil and were flash cooled in liquid nitrogen before data collection.
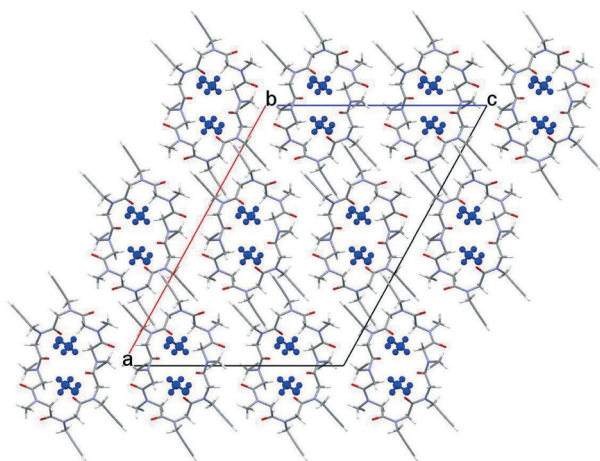
Fig. 12 Crystal packing of form **2A** as viewed along the *b* axis. Methanol molecules are depicted in blue as ball-and-stick.
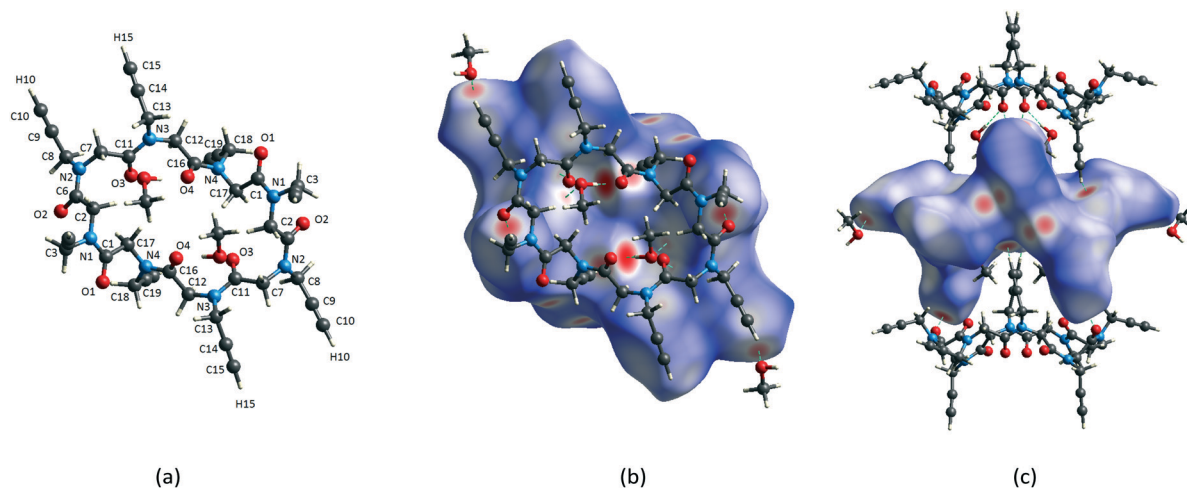
Fig. 13 Hirshfeld surface analysis for the cyclopeptoid molecule in crystal form **2A**. The shortest contacts are depicted as green dotted lines. (a) Cyclopeptoid molecule as viewed along the *b* axis; (b) Hirshfeld surface mapped with d_{norm} as viewed along the *b* axis. The closest cyclopeptoid molecule along the *b* axis is shown as well as the closest methanol molecules; (c) Hirshfeld surface mapped with d_{norm} as viewed along the *c* axis to allow a better view of the closest contacts leading to the formation of the peptoid nanotube.

Single crystal X-ray diffraction

A crystal of **1A** (0.35 mm × 0.015 mm × 0.010 mm) was mounted on a MiTeGen microloop™ and measured at 100 K at the European Synchrotron Radiation Facility beam line ID11. Data reduction was performed with the Bruker package (SMART, Saint, SADABS),[15] Lorentz and polarization corrections were applied to the data.

Crystals of **1B** (0.25 × 0.22 × 0.10 mm) and **2B** (0.32 × 0.15 × 0.12 mm) suitable for laboratory X-ray diffraction were selected and mounted on a MiTeGen microloop™ with Paratone® N oil.

A crystal of **2A** (0.28 × 0.15 × 0.11 mm) suitable for single-crystal X-ray diffraction was selected and mounted on a MiTeGen microloop™ with Paratone® N oil and flash cooled in liquid nitrogen before data collection.

Data collection for **1B**, **2A**, **2B**, **2C** and **2D** were performed at 100 K using a Rigaku AFC7S diffractometer equipped with a Mercury[2] CCD detector using graphite monochromated MoKα radiation (λ = 0.71073 Å). Data reduction was performed with the crystallographic package CrystalClear.[16] Data were corrected for Lorentz, polarization and absorption. The structures were solved by direct methods using the program SIR2011 (ref. 17) in the case of **1A** and SIR2014 (ref. 18) in all other cases and refined by means of full matrix least-squares based on F^2 using the program SHELXL.[19] OLEX2 was used as GUI.[20] Crystal structures were drawn using Mercury.[21]

For all compounds non-hydrogen atoms were refined anisotropically with the exception of the oxygen atoms belonging to water molecules in the hydrate forms **2B**, **2C**, **2D**.

Hydrogen atoms were positioned geometrically and included in structure factor calculations but not refined. In the case of hydrate forms, it was not possible to reliably locate the hydrogen atoms belonging to water molecules.

In forms **2B** and **2D** the methanol molecules are partially substituted by water molecules. The occupancy factors of the oxygen atoms sharing the same site were refined by constraining their sum to 1.0.

In the hydrate form **2C**, inspecting the final difference Fourier map, we were able to locate one of the two crystallographically independent water molecules in two slightly different sites. Disorder was taken into account by refining the oxygen atom coordinates in these two possible sites isotropically and constraining the sum of the occupancies to 1.0. Refinement details are summarized in Tables 1 and 3 respectively for cyclo-(Npa)$_6$ crystal forms (**1A** and **1B**) and cyclo-(Npa)$_8$ crystal forms (**2A**, **2B**, **2C** and **2D**).

Hirshfeld surface analysis

Hirshfeld surface analysis and related fingerprint plots have been performed with Crystal Explorer 3.1.[22]

The Hirshfeld surface arises from the partitioning of the electron density of a crystal into molecular fragments.[23] It provides maximum proximity of neighbouring molecular volumes without volumes overlapping.[24]

d_i is the distance from the surface to the nearest atom interior to the surface. d_e is the distance from the surface to the nearest atom exterior to the surface. d_{norm} is a normalized distance,[25] which takes into account the relative atom sizes:

$$d_{norm} = \frac{d_i - r_i^{vdW}}{r_i^{vdW}} + \frac{d_e - r_e^{vdW}}{r_e^{vdW}}$$

where r^{vdW} is the van der Waals (vdW) radius of the appropriate atom internal or external to the surface.

Relative contributions to the Hirshfeld surface area of particular types of intermolecular contacts are determined by

summing the area corresponding to close contacts between specific types of atoms.[25]

The fingerprint plots summarize quantitatively the nature and type of intermolecular interactions. x and y axes report respectively the d_i and d_e distances.[26]

To compare related structures the lengths of X–H bonds are normalized using standard X–H distances from Allen *et al.*[27] Thus, X–H distances and X···H contacts are not equal to those calculated from the original cif files. As for the crystal form **1B**, the hydrogen atoms belonging to the water molecules were calculated in idealized positions as they could not be located in the Fourier electron density map.

Conclusions

The investigation of the crystal structures of hexameric and octameric propargylated cyclic peptoids provides evidence to the role that ring size plays in the solid state assembly of cyclopeptoids.

Cyclic hexapeptoid **1** gives rise to a layered architecture where guest molecules such as acetonitrile, or water and DMSO molecules intercalate between layers. In compound **2**, by increasing the size of the macrocycle by two (*N*-substituted glycine) residues a tubular architecture is obtained and the guest molecules are able to occupy the void inside of the peptoid nanotube.

The peptoid layers are determined by interannular CO···HC interactions along the short sides of the macrocycles. This assembly mode adds to the list of assembly modes previously reported for cyclic peptoids.

The peptoid nanotubes are determined by the vertical side chains that act as pillars held together by C≡CH···OC hydrogen bonds.

Horizontal side chains act as interlayer or intertube joints that contribute to the stability of the whole solid state assembly.

Guest-exchange experiments allowed us to probe the affinity of the peptoid nanotubes for methanol and/or water molecules.

Acknowledgements

Notes and references

1 J. W. Steed and J. L. Atwood, *Supramolecular Chemistry*, Wiley, 2nd edn, 2013.

2 (*a*) M. L. Lepage, J. P. Schneider, A. Bodlenner, A. Meli, F. De Riccardis, M. Schmitt, C. Tarnus, N.-T. Nguyen-Huynh, Y.-N. Francois, E. Leize-Wagner, C. Birck, A. Cousido-Siah, A. Podjarny, I. Izzo and P. Compain, *Chem. – Eur. J.*, 2016, **22**, 5151–5155; (*b*) R. Schettini, F. De Riccardis, G. Della Sala and I. Izzo, *J. Org. Chem.*, 2016, **81**, 2494–2505; (*c*) C. E. M. Salvador, B. Pieber, P. M. Neu, A. Torvisco, Z. Kleber, C. Andrade and C. O. Kappe, *J. Org. Chem.*, 2015, **80**, 4590–4602; (*d*) T. Hjelmgaard, O. Roy, L. Nauton, M. El-Ghozzi, D. Avignant, C. Didierjean, C. Taillefumier and S. Faure, *Chem. Commun.*, 2014, **50**, 3564–3567; (*e*) F. De Riccardis, C. De Cola, G. Fiorillo, A. Meli, S. Aime, E. Gianolio and I. Izzo, *Org. Biomol. Chem.*, 2014, **12**, 424–431; (*f*) G. Della Sala, B. Nardone, F. De Riccardis and I. Izzo, *Org. Biomol. Chem.*, 2013, **11**, 726–731; (*g*) I. Izzo, G. Ianniello, C. De Cola, B. Nardone, L. Erra, G. Vaughan, C. Tedesco and F. De Riccardis, *Org. Lett.*, 2013, **15**, 598–601; (*h*) S. N. Khan, A. Kim, R. H. Grubbs and Y. U. Kwon, *Org. Lett.*, 2011, **13**, 1582–1585; (*i*) B. Yoo, S. B. Y. Shin, M. L. Huang and K. Kirshenbaum, *Chem. – Eur. J.*, 2010, **16**, 5528–5537; (*j*) J. H. Lee, A. M. Meyer and H. S. Lim, *Chem. Commun.*, 2010, **46**, 8615–8617; (*k*) N. Maulucci, I. Izzo, G. Bifulco, A. Aliberti, C. De Cola, D. Comegna, C. Gaeta, A. Napolitano, C. Pizza, C. Tedesco, D. Flot and F. De Riccardis, *Chem. Commun.*, 2008, 3927–3929; (*l*) Y. U. Kwon and T. Kodadek, *Chem. Commun.*, 2008, 5704–5706; (*m*) S. B. Y. Shin, B. Yoo, L. J. Todaro and K. Kirshenbaum, *J. Am. Chem. Soc.*, 2007, **129**, 3218–3225.

3 For recent reviews see: (*a*) N. Gangloff, J. Ulbricht, T. Lorson, H. Schlaad and R. Luxenhofer, *Chem. Rev.*, 2016, **116**, 1753–1802; (*b*) J. Sun and R. N. Zuckermann, *ACS Nano*, 2013, **7**, 4715–4732; (*c*) I. Izzo, C. De Cola and F. De Riccardis, *Heterocycles*, 2011, **82**, 981–1006; (*d*) A. S. Culf and R. J. Ouellette, *Molecules*, 2010, **15**, 5282–5335.

4 (*a*) G. Angelici, N. Bhattacharjee, O. Roy, S. Faure, C. Didierjean, L. Jouffret, F. Jolibois, L. Perrin and C. Taillefumier, *Chem. Commun.*, 2016, **52**, 4573–4576; (*b*) J. A. Crapster, I. A. Guzei and H. E. Blackwell, *Angew. Chem., Int. Ed.*, 2013, **52**, 5079–5084; (*c*) J. R. Stringer, J. A. Crapster, I. A. Guzei and H. E. Blackwell, *J. Am. Chem. Soc.*, 2011, **133**, 15559–15567; (*d*) S. A. Fowler and H. E. Blackwell, *Org. Biomol. Chem.*, 2009, **7**, 1508–1524; (*e*) B. Yoo and K. Kirshenbaum, *Curr. Opin. Chem. Biol.*, 2008, **12**, 714–721; (*f*) C. W. Wu, K. Kirshenbaum, T. J. Sanborn, J. A. Patch, K. Huang, K. A. Dill, R. N. Zuckermann and A. E. Barron, *J. Am. Chem. Soc.*, 2003, **125**, 13525–13530; (*g*) P. Armand, K. Kirshenbaum, R. A. Goldsmith, S. Farr-Jones, A. E. Barron, K. T. V. Truong, K. A. Dill, D. F. Mierke, F. E. Cohen, R. N. Zuckermann and E. K. Bradley, *Proc. Natl. Acad. Sci. U. S. A.*, 1998, **95**, 4309–4314; (*h*) K. Kirshenbaum, A. E. Barron, R. A. Goldsmith, P. Armand, E. K. Bradley, K. T. V. Truong, K. A. Dill, F. E. Cohen and R. N. Zuckermann, *Proc. Natl. Acad. Sci. U. S. A.*, 1998, **95**, 4303–4308.

5 C. Tedesco, L. Erra, I. Izzo and F. De Riccardis, *CrystEngComm*, 2014, **16**, 3667–3687.

6 (*a*) M. Nishio, Y. Umezawa, J. Fantini, M. S. Weiss and P. Chakrabartie, *Phys. Chem. Chem. Phys.*, 2014, **16**, 12648–12683; (*b*) M. Nishio, Y. Umezawa, K. Honda, S. Tsuboyama and H. Suezawa, *CrystEngComm*, 2009, **11**,

1757–1788; (c) M. Nishio, *CrystEngComm*, 2004, **6**, 130–158; (d) M. Nishio, M. Hirota and Y. Umezawa, *The CH/pi Interaction. Evidence, Nature, and Consequences*, Wiley-VCH, Weinheim, Germany, 1998; (e) G. R. Desiraju and T. Steiner, *The Weak Hydrogen Bond in Structural Chemistry and Biology*, Oxford Science Publication, Oxford, 1999; (f) G. R. Desiraju, *Acc. Chem. Res.*, 1991, **24**, 290–296.

7 Reported values for CO···HC distances and CO···H–C angles in weak hydrogen bonds are respectively within the range 2.2–2.8 Å and 130–160°. Observed values for C···HC distances in CH–pi bonds are within the range 2.6–2.9 Å.

8 (a) D. T. Bong, T. D. Clark, J. R. Granja and M. R. Ghadiri, *Angew. Chem., Int. Ed.*, 2001, **40**, 988–1011; (b) J. D. Hartgerink, J. R. Granja, R. A. Milligan and M. R. Ghadiri, *J. Am. Chem. Soc.*, 1996, **118**, 43–50; (c) M. R. Ghadiri, J. R. Granja, R. A. Milligan, R. E. McRee and N. Khazanovich, *Nature*, 1993, **366**, 324–327.

9 S. B. L. Vollrath, C. Hu, S. Bräse and K. Kirshenbaum, *Chem. Commun.*, 2013, **49**, 2317–2319.

10 (a) G. L. Butterfoss, B. Yoo, J. N. Jaworski, I. Chorny, K. A. Dill, R. N. Zuckermann, R. Bonneau, K. Kirshenbaum and V. A. Voelz, *Proc. Natl. Acad. Sci. U. S. A.*, 2012, **109**, 14320–14325; (b) P. Groth, *Acta Chem. Scand., Ser. A*, 1976, **30**, 840–842; (c) P. Groth, *Acta Chem. Scand., Ser. A*, 1975, **29**, 38–44; (d) P. Groth, *Acta Chem. Scand., Ser. A*, 1977, **31**, 838–840; P. Groth, *Acta Chem. Scand.*, 1973, **27**, 3217–3226; (e) K. Titlestad, P. Roth, J. Dale and M. Y. Ali, *J. Chem. Soc., Chem. Commun.*, 1973, 346–347; (f) P. Groth, *Acta Chem. Scand.*, 1973, **27**, 3419–3426.

11 A. Meli, E. Macedi, F. De Riccardis, V. J. Smith, L. J. Barbour, I. Izzo and C. Tedesco, *Angew. Chem., Int. Ed.*, 2016, **55**, 4679–4682.

12 (a) M. A. Spackman and D. Jayatilaka, *CrystEngComm*, 2009, **11**, 19–32; (b) J. J. McKinnon, D. Jayatilaka and M. A. Spackman, *Chem. Commun.*, 2007, 3814–3816.

13 M. L. Lepage, A. Meli, A. Bodlenner, C. Tarnus, F. De Riccardis, I. Izzo and P. Compain, *Beilstein J. Org. Chem.*, 2014, **10**, 1406–1412.

14 (a) J. L. Crawford, W. N. Lipscomb and C. G. Schellman, *Proc. Natl. Acad. Sci. U. S. A.*, 1973, **70**, 538–542; (b) C. M. Venkatachalam, *Biopolymers*, 1968, **6**, 1425–1436.

15 *Bruker AXS Inc.*, Madison, Wisconsin, USA.

16 *CrystalClear*, Crystal Structure Analysis Package, Rigaku-Molecular Structure Corp.

17 M. C. Burla, R. Caliandro, M. Camalli, B. Carrozzini, G. L. Cascarano, C. Giacovazzo, M. Mallamo, A. Mazzone, G. Polidori and R. Spagna, *J. Appl. Crystallogr.*, 2012, **45**, 339–341.

18 M. C. Burla, R. Caliandro, B. Carrozzini, G. L. Cascarano, C. Cuocci, C. Giacovazzo, M. Mallamo, A. Mazzone and G. Polidori, *J. Appl. Crystallogr.*, 2015, **48**, 306–309.

19 G. M. Sheldrick, *Acta Crystallogr., Sect. C: Struct. Chem.*, 2015, **71**, 3–8.

20 O. V. Dolomanov, L. J. Bourhis, R. J. Gildea, J. A. K. Howard and H. Puschmann, *J. Appl. Crystallogr.*, 2009, **42**, 339–341.

21 C. F. Macrae, I. J. Bruno, J. A. Chisholm, P. R. Edgington, P. McCabe, E. Pidcock, L. Rodriguez-Monge, R. Taylor, J. van de Streek and P. A. Wood, *J. Appl. Crystallogr.*, 2008, **41**, 466–470.

22 S. K. Wolff, D. J. Grimwood, J. J. McKinnon, M. J. Turner, D. Jayatilaka and M. A. Spackman, *CrystalExplorer (Version 3.1)*, University of Western Australia, 2013.

23 (a) M. A. Spackman and D. Jayatilaka, *CrystEngComm*, 2009, **11**, 19–32; (b) J. J. McKinnon, M. A. Spackman and A. S. Mitchell, *Acta Crystallogr., Sect. B: Struct. Sci.*, 2004, **60**, 627–668.

24 M. A. Spackman, *Phys. Scr.*, 2013, **87**, 048103, DOI: 10.1088/0031-8949/87/04/048103.

25 J. J. McKinnon, D. Jayatilaka and M. A. Spackman, *Chem. Commun.*, 2007, 3814.

26 M. A. Spackman and J. J. McKinnon, *CrystEngComm*, 2002, **4**, 378–392.

27 F. H. Allen, O. Kennard, D. G. Watson, L. Brammer, A. G. Orpen and R. Taylor, *International Tables for Crystallography*, ed. A. J. C. Wilson, Kluwer Academic, Dordrecht, 1995, pp. 685–706.